

Majorana edge and end states in planar Josephson junctions

A. P. Garrido,^{1,2,*} P. A. Orellana,¹ and A. Matos-Abiague²

¹*Department of Physics, Technical University Federico Santa María, Valparaíso, Valparaíso 2390123, Chile.*

²*Department of Physics and Astronomy, Wayne State University, Detroit, Michigan 48201, USA.*

(Dated: February 25, 2025)

We theoretically investigate the localization properties of Majorana states (MSs) in proximitized, planar Josephson Junctions (JJs) oriented along different crystallographic orientations and in the presence of an in-plane magnetic field and Rashba and Dresselhaus spin-orbit couplings. We show that two types of MSs may emerge when the junction transits into the topological superconducting state. In one case, referred to as end-like MSs, the Majorana quasiparticles are mainly localized inside the normal region at the opposite ends of the junction. In contrast, edge-like MSs extend along the opposite edges of the system, perpendicular to the junction channel. We show how the MSs can transit from end-like to edge-like and vice versa by tuning the magnetic field strength and/or the superconducting phase difference across the junction. In the case of phase-unbiased JJs the transition may occur as the ground state phase difference self-adjusts its value when the Zeeman field is varied.

I. INTRODUCTION

Majorana states (MSs) are zero-energy quasiparticle excitations predicted to appear localized at the boundaries of topological superconductors (TSCs) [1–6]. The MSs obey a non-Abelian exchange statistic, which makes them promising candidates for realizing robust qubits with potential applications in fault-tolerant quantum computing [7–10].

Topological superconductivity (TS) can be engineered by using semiconductor nanowires with large spin-orbit coupling (SOC) and proximitized by s-wave superconductors [11–21], proximitized systems exposed to magnetic textures [22–32], and magnetic chains on s-wave superconductors [33–38]. Proximitized planar JJs have recently emerged as promising platforms for creating and manipulating MSs [39–65]. In addition to the experimental advances in building such structures, proximitized planar JJs have also been shown to possess an enhanced parameter space supporting the topological superconducting state [40, 66].

Magnetic and crystalline anisotropic effects have been predicted to appear in the Josephson junction with non-centrosymmetric materials [67–70]. In particular, it has been shown that in the presence of SOC the Zeeman interaction yields a strong dependence of the system properties on the magnetic field direction. Furthermore, in systems with Rashba [71] and Dresselhaus [72] SOC the crystallographic orientation can affect the topological superconducting state, its robustness, and signatures [67, 68, 73].

Most previous investigations of TS in planar JJs have focused on *end* MSs, i.e., MSs that localize at the opposite ends of the junction with short localization lengths both along the junction (\hat{y} direction, as shown in Fig. 1) and along the system edges perpendicular to the junction (\hat{x} direction, as shown in Fig. 1) [53, 57, 67, 68, 74].

However, theoretical evidence of the existence of *edge* MSs (i.e., MSs that are localized along the junction direction but spread along the entire system edges perpendicular to the junction) has been provided in previous works [46, 67, 75]. The formation of MSs exhibiting anomalous multilocality in three-terminal Josephson junctions has also been proposed [76]. Besides JJs, Majorana edge states can also emerge in hybrid superconductor/ferromagnet structures with helical magnetic textures [77]. Moreover, two-dimensional structures, typically associated with quantum anomalous Hall systems coupled to superconductors, have been shown to support chiral Majorana edge states [78–80] flowing around the sample edges in opposite directions and Majorana corner modes localized at vertices [81–83].

In this work, we study the formation and properties of edge-like and end-like MSs in proximitized planar JJs and characterize them by introducing a quantity (here referred to as the topological gap character) that contains information about the topological charge, topological gap, and the localization nature of the zero-energy states. The norm of the topological gap character determines the size of the topological gap relative to the proximity-induced superconducting gap, and its sign indicates whether the system is in a TS state with *edge*-like (positive sign) or *end*-like (negative sign) MSs. We analyze how the localization character of MSs depends on relevant system parameters such as the magnetic field strength and direction, the superconducting phase difference across the junction, the SOC strength, and the junction crystallographic orientation. Moreover, our study reveals the possibility of inducing transitions from end-like to edge-like MSs (and vice versa) by tuning the magnetic field strength and/or the superconducting phase difference. In phase-unbiased JJs, the transition between end-like and edge-like MSs may occur as the ground state phase difference self-adjusts its value when the Zeeman field is varied. The paper is organized as follows. Section II presents the theoretical model and an overview of the relevant quantities used for characterizing the systems

* alejandro.garridoh@usm.cl

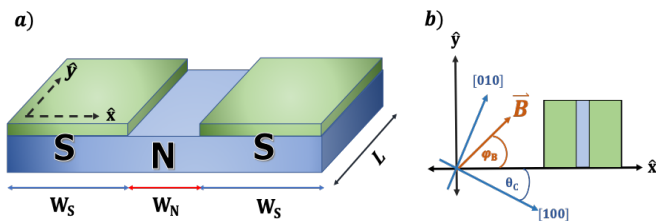


FIG. 1. (a) Schematic of a JJ consisting of a noncentrosymmetric semiconductor 2DEG (blue) in contact with two superconducting (S) leads (green). The \hat{x} and \hat{y} axes define the coordinate system in the junction's reference frame. A top gate (not shown) over the normal (N) region can be used to modulate the Rashba SOC strength [48, 84]. (b) Relevant angles in the junction coordinate system: φ_B defines the direction of the in-plane magnetic field (\mathbf{B}) with respect to the \hat{x} axis, while θ_c determines the orientation of the junction reference frame with respect to the semiconductor's [100] crystallographic axis.

and the MSs. The numerical simulations and main results are discussed in Sec. III, while concluding remarks are given in Sec. IV.

II. THEORETICAL MODEL

We consider a planar JJ composed of a 2D electron gas (2DEG) formed in a noncentrosymmetric semiconductor and subject to an in-plane magnetic field \mathbf{B} . The superconducting (S) regions are induced in the 2DEG by proximity to the superconducting cover layers, while the uncovered region remains in the normal (N) state [Fig. 1(a)]. Excitations in the JJ are described by the Bogoliubov-de Gennes (BdG) Hamiltonian,

$$H = \tau_z \otimes H_0 + \tau_0 \otimes \mathbf{E}_z \cdot \boldsymbol{\sigma} + \Delta(x)\tau_+ + \Delta^*(x)\tau_- , \quad (1)$$

where

$$H_0 = \left[\frac{\mathbf{p}^2}{2m^*} + V(x) - (\mu_S - \varepsilon) \right] \sigma_0 + \frac{\alpha}{\hbar} (p_y \sigma_x - p_x \sigma_y) + \frac{\beta}{\hbar} [(p_x \sigma_x - p_y \sigma_y) \cos 2\theta_c - (p_x \sigma_y + p_y \sigma_x) \sin 2\theta_c]. \quad (2)$$

Here σ_0 and τ_0 are unit matrices, $\sigma_{x,y,z}$ and $\tau_{x,y,z}$ denote the Pauli matrices in particle-hole and spin spaces, respectively. The linear momentum is represented by \mathbf{p} , m^* is the electron effective mass, $\tau_{\pm} = (\tau_x \pm i\tau_y) \otimes \sigma_0/2$, and $V(x) = (\mu_S - \mu_N)\Theta(W_N/2 - |x|)$ describes the difference between the chemical potentials in the N (μ_N) and S (μ_S) regions. The Rashba and Dresselhaus SOC strengths are represented by α and β , respectively. The angle θ_c characterizes the orientation of the junction with respect to the crystallographic direction [100] of the semiconductor [Fig. 1-(b)]. The chemical potentials are measured with respect to the minimum of the single-particle energies, $\varepsilon = m^*\lambda^2(1 + |\sin 2\theta_c|)/2\hbar^2$. Here we use the SOC parametrization,

$$\alpha = \lambda \cos \theta_{so}, \quad \beta = \lambda \sin \theta_{so}, \quad \lambda = \sqrt{\alpha^2 + \beta^2}, \quad (3)$$

where λ represents the overall strength of the combined Rashba and Dresselhaus SOCs, while the spin-orbit angle,

$$\theta_{so} = \text{arccot}(\alpha/\beta). \quad (4)$$

characterizes the relative strength between them.

The second term in Eq. (1) corresponds to the Zeeman interaction and is determined by the vector,

$$\mathbf{E}_z = -\frac{g^* \mu_B B}{2} (\cos \varphi_B, \sin \varphi_B, 0)^T. \quad (5)$$

with g^* , μ_B , B , and φ_B representing the effective g -factor, the Bohr magneton, the magnetic field strength, and the magnetic field direction, respectively. In what

follows, we use $E_Z = g^* \mu_B B/2$ to denote the amplitude of the Zeeman energy. The spatial dependence of the superconducting gap is,

$$\Delta(x) = \Delta_0 e^{i \text{sgn}(x)\phi/2} \Theta(|x| - W_N/2), \quad (6)$$

where ϕ is the phase difference across the JJ and Δ_0 is the magnitude of the proximity-induced superconducting gap.

A. Topological charge

To identify the topological regions we investigate how different sets of system parameters affect the topological invariants characterizing the junction. The presence of the magnetic field breaks the time-reversal invariance and the system generically belongs to the D class, characterized by the topological charge (i.e., the \mathbb{Z}_2 topological index),

$$Q = \text{sgn} \left[\frac{\text{Pf}\{H(k_y = \pi)\tau_y \otimes \sigma_y\}}{\text{Pf}\{H(k_y = 0)\tau_y \otimes \sigma_y\}} \right], \quad (7)$$

where $\text{Pf}\{\dots\}$ denotes the Pfaffian [85–88]. The topological charge determines whether a system belonging to the D class is in a trivial ($Q = 1$) or topological ($Q = -1$) phase [89–94].

It is worth noting that under some conditions determined by the SOC field, the magnetic field direction, and the junction crystallographic orientation, symmetric junctions may effectively belong to the BDI class [67].

In such cases, the topological phases are characterized by the \mathbb{Z} topological invariant of the BDI class. Since the topological charge Q is determined by the parity of the \mathbb{Z} index, the topologically non-trivial regions of the BDI class consist of non-trivial D-class regions (composed of odd \mathbb{Z} index subregions) enhanced by regions with even \mathbb{Z} index [40, 43]. We found that the topological gap in BDI class regions with multiple pairs of MSs is relatively small in the systems considered here. Therefore, our investigation focuses on regions that support only a single pair of MSs. The extent of these regions can be determined by examining how the topological charge Q depends on the system parameters.

B. Topological gap

As the system transits into the topological state, MSs emerge as pairs of degenerate zero-energy states which are isolated from the rest of the excitation spectrum by the energy gap, Δ_{top} , referred to as the topological gap and defined as,

$$\Delta_{top} = (E_1 - E_0). \quad (8)$$

Here E_0 and E_1 are the two lowest-energy states on the positive branch of the energy spectrum, respectively. Due to finite-size effects, the MSs localized at opposite ends (or edges) may overlap, so their energy ($\pm E_0$) may slightly deviate from zero. Note that Eq. (8) can only be interpreted as the topological gap when the system is in the TS state.

In the topological superconducting (TS) state, the topological gap protects the Majorana bound states (MS) from smooth local perturbations. However, the degree of protection depends on the size of the topological gap, as the information stored in the MS can be compromised if the perturbation energy approaches or exceeds Δ_{top} . Thus, large values of Δ_{top} are desirable for designing robust MSs suitable for constructing fault-tolerant qubits.

The magnitude of Δ_{top} has been shown to strongly depend on the junction's crystallographic orientation (θ_c), the spin-orbit angle (θ_{so}) and the in-plane magnetic field orientation (φ_B), being optimal when the following relation is fulfilled [67, 68],

$$\tan \varphi_B = \cot \theta_{so} \sec 2\theta_c - \tan 2\theta_c. \quad (9)$$

Therefore, it is crucial to investigate how the topological gap protecting the end-like and edge-like MSs depends on the superconducting phase difference and magnetic field strength in junctions subjected to the constraint imposed by Eq. (9).

C. End-like vs. edge-like Majorana states

As briefly discussed in the Introduction, end-like MSs are localized at the opposite ends of the junction channel, with short localization lengths both along the junction and along the system's edges perpendicular to it. In contrast, edge-like MSs are localized solely along the junction direction but extend across the full length of the system's edges perpendicular to the junction. We want to emphasize that the edge-like MSs examined here differ from both chiral Majorana states commonly associated with quantum anomalous Hall systems coupled to superconductors [78–80] and unidirectional Majorana edge states in noncentrosymmetric superconductors [95].

To understand the origin of the extended nature of edge-like MSs, consider a simplified model of a junction sufficiently long such that the overlap between Majorana states at opposite edges is negligible. In this scenario, we can focus solely on one Majorana state, for instance, the one localized at the bottom edge ($y = 0$). Assuming the S regions are infinitely wide ($W_S \rightarrow \infty$), the scattering states in the left S region can be expressed as [67, 73],

$$\Psi(\mathbf{r}) = e^{-\kappa y} \sum_{s=\pm} [C_{e,s} \chi_{e,s} e^{-iq_{e,s}x} + C_{h,s} \chi_{h,s} e^{iq_{h,s}x}], \quad (10)$$

where κ describes the localization of the Majorana state along the junction y -direction, the subindexes e and h refer to electron-like and hole-like states, respectively, $s = \pm$ characterizes the spin, and $q_{e,s}$ ($q_{h,s}$) is the wave vector of the electron-like (hole-like) state with spinor $\chi_{e,s}$ ($\chi_{h,s}$) and spin s .

At $\phi = 0$, the coefficients $C_{e,s}$ and $C_{h,s}$ become phase-independent, and the asymptotic behavior of $\Psi(x, y)$ along the edge is entirely determined by the wave vectors. By combining Eqs. (1) and (10) and requiring the energy to vanish, we obtain the following quartic equation for q^2 ,

$$(|\mathbf{E}_Z|^2 + \mathbf{w} \cdot \mathbf{w} + |\Delta_0|^2 + \xi^2)^2 - 4 [|\mathbf{E}_Z|^2 (|\Delta_0|^2 + \xi^2) + (\mathbf{w} \cdot \mathbf{w}) \xi^2 + (\mathbf{E}_z \cdot \mathbf{w})^2] = 0, \quad (11)$$

where,

$$\mathbf{w} = \begin{pmatrix} q\beta \cos 2\theta_c + i\kappa(\alpha - \beta \sin 2\theta_c) \\ -q(\alpha + \beta \sin 2\theta_c) - i\kappa\beta \cos 2\theta_c \\ 0 \end{pmatrix}, \quad (12)$$

is the spin-orbit field and $\xi = \hbar^2 q^2 / (2m^*) - \mu_S + \epsilon$.

The solutions to the quartic equation [Eq. (11)] represent the wave vectors $q_{j,s}$ ($j = e, h$). At $\phi = 0$, the Majorana state's character is determined by the nature of these wave vectors. Specifically, each scattering mode $\{j, s\}$

contributing to the Majorana state in the S region decays within a characteristic length,

$$l_{j,s} \sim \frac{1}{\text{Im}[q_{j,s}]} . \quad (13)$$

The overall localization length of the Majorana state along the edge is given by the largest of the $l_{j,s}$. Hence, at $\phi = 0$, end-like Majorana states appear when all wave vectors are complex. Conversely, if at least one wave vector is purely real, the corresponding scattering mode represents a propagating wave, leading to an edge-like MS.

The coefficients of the quartic equation [Eq. (11)] are generally complex, yielding complex solutions for all wave vectors and resulting in end-like MSs. However, if the conditions,

$$\alpha^2 \sin 2\varphi_B + \beta^2 \sin(2\varphi_B + 4\theta_c) = \alpha\beta \cos 2\theta_c = 0, \quad (14)$$

are satisfied, all coefficients of the quartic equation become real. This allows for purely real wave vectors, enabling the emergence of edge-like MSs if the system parameters are appropriately tuned. All the configurations considered in the numerical analysis presented in Sec. III are chosen in such a way that Eq. (14) and the condition for optimal topological gap [Eq. (9)] are simultaneously fulfilled.

In general, we can anticipate three scenarios: i) four real wave vectors, leading to edge-like MSs composed of the superposition of four propagating modes; ii) two real and two complex wave vectors, resulting in edge-like MSs formed by two propagating and two localized modes; and iii) four complex wave vectors, corresponding to localized end-like MSs. By appropriately tuning the system parameters, the system can be driven into any of these scenarios, enabling controlled transitions between end-like and edge-like behaviors. Furthermore, at finite superconducting phase differences, the coefficients $C_{e,s}$ and $C_{h,s}$ in Eq. (10) become ϕ -dependent. This dependence governs the interference between the four scattering modes, thereby modulating the localization characteristics of the Majorana states (MSs).

To capture the topological character of the state, the magnitude of the topological gap, and the extension of the MSs along the edges perpendicular to the junction, we introduce the quantity,

$$\tilde{\Delta} = \frac{(1-Q)\Delta_{top}}{2\Delta_0} \text{sgn}(\xi) \quad (15)$$

where ξ is a parameter that characterizes the nature of the MSs, taking positive values for edge-like MSs and negative values for end-like MSs.

In what follows, we refer to $\tilde{\Delta}$ as the *topological gap character*. Its magnitude represents the topological gap normalized to the proximity-induced superconducting gap, while its sign indicates the nature of the Majorana states: positive for edge-like MSs, negative for end-like MSs, and zero when the system is in the trivial state (or

in the BDI-class TS with an even number of Majorana pairs), i.e.,

$$\tilde{\Delta} = \begin{cases} +\Delta_{top}/\Delta_0 & \text{for D-class TS with edge-like MSs} \\ 0 & \text{for trivial phase with no MSs} \\ 0 & \text{for even BDI-class TS phase} \\ -\Delta_{top}/\Delta_0 & \text{for D-Class with end-like MSs} \end{cases} . \quad (16)$$

Although we limit our analysis to MSs within the D class, the topological character defined in Eq. (15) can easily be generalized to account for the BDI-class TS by using the winding number (the \mathbb{Z} topological invariant) instead of the topological charge.

For the junctions studied here, the probability density of edge-like MSs displays an oscillatory behavior along the edge, with multiple local maxima of comparable amplitudes. In contrast, the probability density oscillations of end-like MSs decay rapidly, featuring a large maximum at the middle of the junction edge, followed by a few significantly smaller maxima. Therefore, the localization nature of the MSs can be captured by the parametrization $\xi = n - n_0 - 1/2$, where n is the number of probability density local maxima with comparable amplitudes. Since the typical number of local maxima for end-like MSs is smaller than 3, we set $n_0 = 3$ in the numerical simulations of Eq.(16) discussed below. For higher chemical potentials and/or larger W_N and W_S one may need to increase n_0 accordingly.

D. Phase-biased and phase-unbiased JJs

The eigenenergies E_n can be used to compute the phase-dependent part of the junction's free energy,

$$F = - \sum_{E_n > 0} [E_n + 2k_B T \ln(1 + e^{-E_n/k_B T})]. \quad (17)$$

In the phase-biased case, the JJ is incorporated in a closed loop threaded by a magnetic flux Φ , which fixes the superconducting phase across the junction to $\phi = 2\pi\Phi/\Phi_0$, where Φ_0 is the magnetic flux quantum.

In the absence of the magnetic flux, the junction is phase unbiased, and the phase difference is self-adjusted in such a way that the free energy of the system is minimized. The ground-state phase (ϕ_{GS}) is the superconducting phase difference that minimizes the free energy of the system, i.e.,

$$F(\phi_{GS}) = \min_{\phi} F(\phi). \quad (18)$$

Since the free energy also depends on the Zeeman energy, ϕ_{GS} is generally a function of the magnetic field. This offers a mechanism for indirectly controlling the superconducting phase difference using an in-plane magnetic field, without relying on a magnetic flux.

III. RESULTS

We consider two types of junctions: (i) Al/HgTe Josephson junctions (JJs), where Rashba spin-orbit coupling (SOC) is the dominant effect, and (ii) Al/InSb JJs, where both Rashba and Dresselhaus SOC may be significant. The system parameters used in our calculations are provided in Appendix A. The numerical simulations were carried out by discretizing Eq. (1) on a mesh with a lattice constant of $a = 10$ nm. Using the finite-difference approximation, we constructed the tight-binding (TB) form of the BdG Hamiltonian with the Kwant package [96]. The energy spectrum and wave functions were obtained by numerically diagonalizing the TB BdG Hamiltonian on a finite lattice. The energy spectrum was then used to compute the topological gap [Eq. (8)], the phase-dependent part of the free energy [Eq. (16)], and the ground-state phase [Eq. (16)]. The topological charge [see Eq. (7)] was computed by using the system TB BdG Hamiltonian with imposed translational invariance along the junction direction.

A. Effects of Rashba SOC

In Al/HgTe Josephson junctions (JJs), where Rashba SOC is the dominant and Dresselhaus SOC is negligibly small (i.e., $\beta \approx 0$), the spin-orbit angle $\theta_{so} \approx 0$ and $\lambda \approx \alpha$ [see Eqs. (3) and (4)]. In this scenario, the system exhibits magneto anisotropy (i.e., its properties depend on the in-plane magnetic field orientation, φ_B), while crystalline anisotropy is absent (i.e., the system properties are independent of the junction's crystallographic direction, θ_c) [66–68]. For the calculations presented in this subsection, the in-plane magnetic field was aligned with the junction direction (i.e., $\varphi_B = \pi/2$), which, as discussed in Ref. [67], yields the optimal topological gap for this configuration.

Figure 2(a) shows the behavior of the topological gap character ($\tilde{\Delta}$), as a function of the Zeeman field (E_Z) and the superconducting phase difference (ϕ) in a phase-biased JJ. Gray areas correspond to $\tilde{\Delta} = 0$, indicating topologically trivial (with respect to the D classification) regions with topological charge $Q = 1$. Note, however, that the gray zone may still contain regions of BDI-class TS with an even number of MS pairs. As previously mentioned here we disregard those regions, as they exhibit a relatively small topological gap. Blue (red) areas indicate regions where $\tilde{\Delta} < 0$ ($\tilde{\Delta} > 0$) correspond to a D-class TS phase that supports the formation of end-like (edge-like) MSs. The figure reveals that in junctions where only Rashba SOC is significant, the formation of end-like MSs with a sizable topological gap is favored for ϕ -values near π . In contrast, less robust edge-like MSs with smaller topological gaps emerge when the system is in the TS state, and ϕ is near 0 or 2π .

The effect of the superconducting phase difference on

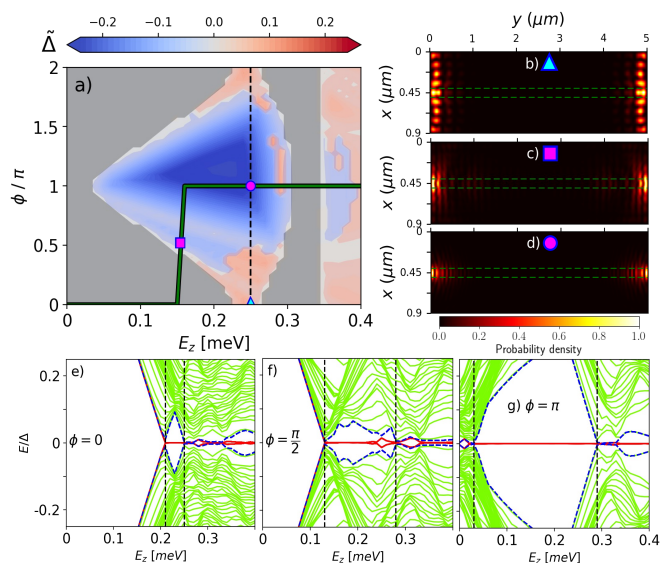


FIG. 2. (a) Topological gap character ($\tilde{\Delta}$) as a function of the Zeeman energy E_Z and the superconducting phase difference (ϕ) across an Al/HgTe JJ with only Rashba SOC ($\theta_{so} = 0$). The junction and magnetic field orientations are set to $\theta_c = 0$ and $\varphi_B = \pi/2$, respectively. The green solid line represents the path of the ground-state phase (ϕ_{GS}) as the Zeeman energy is varied. The vertical dashed line marks a possible transition between a TS state supporting a zero-phase edge-like MS (cyan triangle) and one supporting an end-like MS (magenta dot) during which E_Z is kept constant, while ϕ is tuned. (b)-(d) Probability density (normalized to its maximum value) of the MSs corresponding to the E_Z and ϕ values marked in (a) by the cyan triangle (edge-like MS), magenta square (end-like MS), and magenta dot (end-like MS), respectively. (e)-(g) Energy spectra as a function of the Zeeman energy for $\phi = 0$, $\phi = \pi/2$, and $\phi = \pi$, respectively. Red-solid and dashed-blue lines represent states that evolve into MSs as E_Z is varied. Vertical dashed lines indicate the boundaries of the first topological region in which only a single pair of MSs (red solid lines) exists.

the localization nature of the MSs can be qualitatively understood by noting that the phase factor of the superconducting pairing potential appearing in the antidiagonal blocks of the BdG Hamiltonian can be gauged away by a position-dependent unitary transformation (see details in Appendix B). As a result, the BdG Hamiltonian of a junction with a superconducting phase difference ϕ is transformed into a BdG Hamiltonian of a junction with zero phase difference, but in the presence of a position-dependent gauge potential with strength proportional to ϕ . The edge-like MSs at zero phase transit to end-like MSs when the ϕ -dependent gauge field is strong enough.

Considering a junction with infinitely wide S regions (i.e., $W_S \rightarrow \infty$) and a Zeeman field along the junction direction and much larger than the Rashba SOC splitting, we can write the approximate solutions of Eq. (11)

as,

$$q_{j,s} = \sqrt{\left[\frac{\sqrt{2m^* (\mu_S + j\sqrt{E_Z^2 - \Delta_0^2})}}{\hbar} + s k_{so} \right]^2 + \kappa^2} \quad (19)$$

where $j = e = 1$ ($j = h = -1$) for electron-like (hole-like) states, $E_Z = |\mathbf{E}_Z|$, and $k_{so} = m^* \alpha / \hbar^2$. This indicates that zero-phase edge-like MSs of junctions with only Rashba SOC and magnetic field along the junction direction appear when the system is in the TS state and the following conditions are fulfilled,

$$E_Z \geq \Delta_0 \text{ and } \mu_S \geq \sqrt{E_Z^2 - \Delta_0^2}. \quad (20)$$

Indeed, in such a situation, all the wave vectors are purely real (i.e. $\text{Im}[q_{j,s}] = 0$) and the MS localization length, $l_{j,s} \rightarrow \infty$.

When the second inequality in Eq.(20) is satisfied (as it is for the parameters used in the numerical simulations), the emergence of edge-like MSs at $\phi = 0$ in the limit $W_S \rightarrow \infty$ is governed by the condition $E_Z \geq \Delta_0$. However, since the numerical simulations account for superconducting regions of finite width, the results shown in Fig. 2(a) —where zero-phase edge-like MSs appear at Zeeman energies slightly below Δ_0 —exhibit a small deviation from the condition $E_Z \geq \Delta_0$. The impact of finite-size effects on the topological phase diagram of planar JJs has been explored in Ref.[66].

In phase-unbiased junctions, the system's state evolves according to the trajectory of the ground-state phase [see green solid line in Fig. 2(a)] as the Zeeman field is varied. During the $0 - \pi$ ground-state jump at $E_Z \approx 0.14$ meV, the junction undergoes a transition from the trivial to a TS phase with end-like MSs. A self-tuning mechanism, where edge-like MSs transition into end-like MSs (and/or vice versa) as the Zeeman field varies, appears impractical in phase-unbiased junctions with only Rashba SOC. However, a topologically protected transition in which end- and edge-like MSs can be transformed into each other without exiting the TS state seems feasible by tuning the magnetic flux in phase-biased Josephson junctions (JJs). Since the system remains in the same TS state the topological gap does not close during the process, providing topological protection to the transition. This is illustrated in Fig. 2(a), where an edge-like MS (cyan triangle) can evolve into an end-like MS (magenta dot) by adjusting the Zeeman field (at the value indicated by the vertical dashed line) and varying the phase from 0 to π .

To visualize the spatial extension of the edge-like MSs along the sample edges perpendicular to the junction, Fig. 2(b) shows the probability density (normalized to its maximum value) of the edge-like MS corresponding to the cyan triangle in Fig. 2(a) at $\phi = 0$. The probability density exhibits an oscillatory behavior with multiple maxima of comparable amplitude. Note that the edge-like MSs consistently spread along the entire exten-

sion, regardless of the width W_S of the S regions (see Appendix C). In contrast, the probability density of the end-like MSs corresponding to the magenta square and magenta dot in Fig. 2(a) [see Figs. 2(c) and (d), respectively] is localized at the opposite ends of the junction with wave functions that decay both along and perpendicular to the junction's direction.

The energy spectrum as a function of E_Z is shown in Figs. 2(e)-(g) for $\phi = 0, \pi/2, \pi$, respectively. The red solid and blue dotted lines represent the states with energies closest to zero, which evolve into MS as the junction transitions into the TS phase. The vertical lines mark the Zeeman energy boundaries of the first topological region, characterized by the \mathbb{Z}_2 invariant of the D class, where the topological charge is $Q = -1$ [see Eq. (7)]. Within this region, the absolute value of the \mathbb{Z} invariant of the BDI class equals 1, indicating the presence of a single pair of MSs, as shown by the red lines in Figs. 2(e)-(g). Additionally, regions where a second pair of MSs emerge (blue dashed lines) can also be observed. In these regions, the system remains in the BDI class and supports two pairs of MSs, corresponding to an absolute value of 2 for the \mathbb{Z} invariant of the BDI class. However, it is important to note that the topological gap in regions with multiple pairs of MSs is significantly smaller than in regions where only a single pair of MSs exists [this is particularly clear in Fig. 2(g)]. For this reason, our analysis of edge-like and end-like MSs is focused on topological regions containing only a single pair of MSs.

B. Effects of Dresselhaus SOC

We now focus on JJs where only the Dresselhaus SOC plays a significant role. In this scenario, with $\alpha = 0$ and $\lambda = \beta \neq 0$, we can assume $\theta_{so} = \pi/2$ without loss of generality. Unlike linear Rashba SOC, the Dresselhaus spin-orbit field is not rotationally invariant about the axis normal to the junction plane, leading to the emergence of both magneto-anisotropy and crystalline anisotropy in the system. Therefore, to optimize the topological gap, it is essential to carefully align both the in-plane magnetic field angle φ_B and the crystallographic orientation of the junction θ_c . For numerical simulations, we use the values $\theta_c = \varphi_B = 0$, which together with $\theta_{so} = \pi/2$, satisfy the condition in Eq. (9).

The character of the topological gap $\tilde{\Delta}$, depicted in Fig. 3(a) as a function of E_Z and ϕ , exhibits an overall behavior similar to that shown in Fig. 2(a). Specifically, edge and end-like MSs emerge at phase values near 0 and π , respectively. Notably, edge-like MSs are better protected by a larger topological gap in JJs dominated by Dresselhaus SOC compared to those where Rashba SOC is predominant.

The ground-state phase trajectory [green line in Fig. 2(a)] in phase-unbiased JJs undergoes a $0 - \pi$ transition, enabling the system to enter the TS state at a lower Zeeman energy compared to when the phase is fixed at

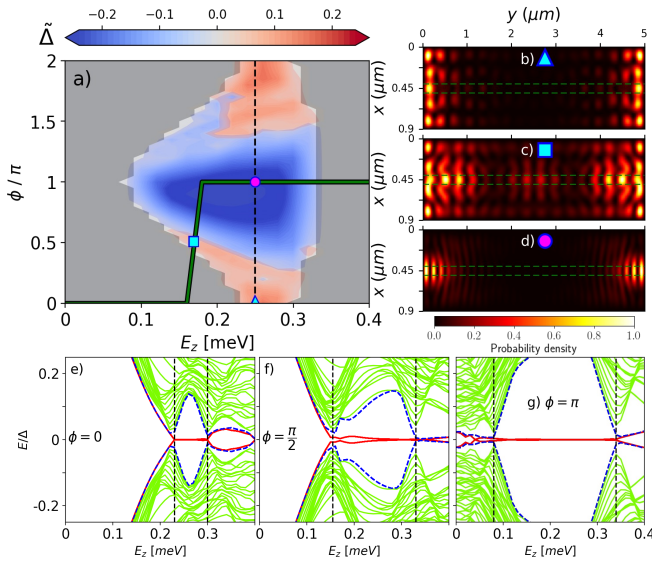


FIG. 3. (a) Topological gap character ($\tilde{\Delta}$) as a function of the Zeeman energy E_Z and the superconducting phase difference (ϕ) across an Al/InSb JJ, where the Rashba SOC has been tuned to a negligibly small value and only Dresselhaus SOC is relevant ($\theta_{so} = \pi/2$). The junction and magnetic field orientations are set to $\theta_c = 0 = \varphi_B = 0$. The green solid line represents the path of the ground-state phase (ϕ_{GS}) as the Zeeman energy is varied. The vertical dashed line marks a possible transition between a TS state supporting a zero-phase edge-like MS (cyan triangle) and one supporting an end-like Majorana state (magenta dot) during which E_Z is kept constant, while ϕ is tuned. (b)-(d) Probability density (normalized to its maximum value) of the MSs corresponding to the E_Z and ϕ values marked in (a) by the cyan triangle (edge-like MS), cyan square (edge-like MS), and magenta dot (end-like MS), respectively. (e)-(g) Energy spectra as a function of the Zeeman energy for $\phi = 0$, $\phi = \pi/2$, and $\phi = \pi$, respectively. Red-solid and dashed-blue lines represent states that evolve into MSs as E_Z is varied. Vertical dashed lines indicate the boundaries of the first topological region in which only a single pair of MSs (red solid lines) exists. The deviation of the edge-like MS energies (red solid lines) from zero in (f) results from the wavefunction overlap between edge-like MSs on opposite edges [see (c)].

zero. However, as in the case of Rashba SOC, a self-tuned transition from end-like to edge-like MSs appears unfeasible in JJs with only Dresselhaus SOC. Nonetheless, the end-to-edge transition can still be achieved with external control of the superconducting phase difference. For example, as indicated by the vertical dotted line in Fig. 3(a), fixing the in-plane magnetic field to a value corresponding to $E_Z \approx 0.25$ meV and tuning ϕ from 0 to π would induce a transition from edge to end-like MSs.

The probability density of MSs corresponding to the values of E_Z and ϕ marked by the cyan triangle, cyan square, and magenta dot in Fig. 3(a) are shown in Figs. 3(b)-(d), respectively. Additionally, the dependence of the energy spectra on E_Z for $\phi = 0, \pi/2, \pi$ is depicted in Figs. 3(e)-(g), respectively. Compared to the edge-like

MS illustrated in Fig. 2(b), the zero-phase edge-like MSs in Fig. 3(b) are protected by a larger topological gap [see Figs. 2(e) and 3(e)]. However, MSs in junctions with only Rashba SOC exhibit stronger localization along the junction, implying that JJs with dominant Dresselhaus SOC would need to be longer to effectively prevent the overlap between MSs localized at opposite ends (or edges). The overlap between MSs from opposite edges, particularly evident in Fig. 3(c), causes their energies to deviate from zero [seen in Fig. 3(f)].

C. Effects of combined Rashba and Dresselhaus SOCs

In systems like Al/InSb-based junctions, the coexistence of significant Rashba and Dresselhaus SOC generates a two-fold symmetric spin-orbit field. This, combined with the Zeeman interaction, results in nontrivial magneto anisotropic and crystalline anisotropic effects. The relative strength of Rashba (α) and Dresselhaus (β) SOCs can be tuned by adjusting the Rashba SOC via a gate placed on top of the junction [48]. A particularly interesting regime arises when the Rashba and Dresselhaus SOCs are equally strong. Based on the parametrization introduced in Eqs. (3) and (4), the condition $\alpha = \beta$ corresponds to the SOC angle $\theta_{so} = \pi/4$.

The character of the topological gap ($\tilde{\Delta}$) is shown in Fig. 4(a) as a function of E_Z and ϕ , with $\theta_{so} = \pi/4$. The crystallographic and magnetic field orientations were chosen as $\theta_c = 3\pi/4$ and $\varphi_B = \pi/2$, respectively, ensuring that the condition in Eq. (9) is satisfied. A distinctive feature of this regime is that, unlike the previously discussed cases, edge-like MSs can emerge at superconducting phase differences close to π . Additionally, the coexistence of Rashba and Dresselhaus SOCs leads to an overall enhancement of the topological gap.

As in the cases discussed in the previous subsections, in phase-biased JJs with both Rashba and Dresselhaus SOC transitions between edge and end-like MSs can also be induced by tuning the magnetic field while keeping the phase fixed at an appropriate value [e.g., following the dotted line from the cyan dot to the magenta square in Fig. 4(a)] or by fixing the magnetic field and tuning the phase difference [e.g., following the dotted line from the cyan triangle to the magenta square in Fig. 4(a)]. Remarkably, the coexistence of Rashba and Dresselhaus SOC allows for transitions between edge and end-like MSs in phase-unbiased junctions, something not observed in systems with only Rashba or only Dresselhaus SOC. As shown in Fig. 4(a), the self-tuning of the ground-state phase (green solid line) as the Zeeman energy varies creates a transition pathway between (red) regions hosting edge-like MSs and (blue) regions hosting end-like MSs. For instance, along the ground-state trajectory, the edge-like MSs at the cyan dot can transition into the end-like MSs at the magenta cross.

For completeness, the probability densities of the MSs

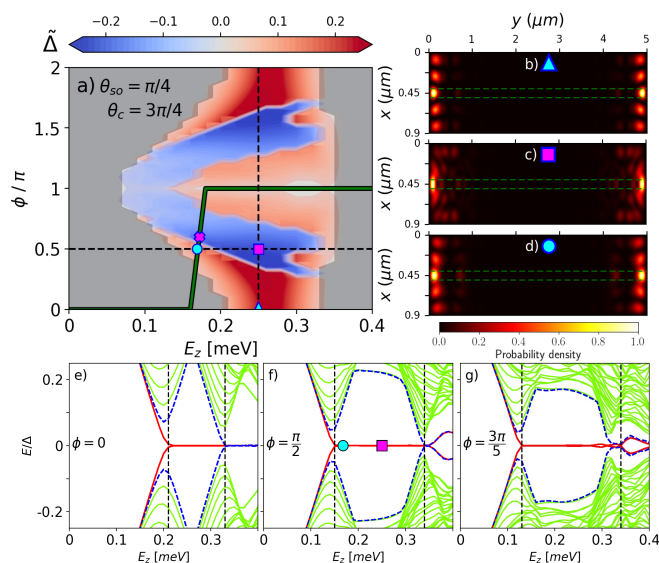


FIG. 4. (a) Topological gap character ($\tilde{\Delta}$) as a function of the Zeeman energy E_Z and the superconducting phase difference (ϕ) across an Al/InSb JJ, with equal Rashba and Dresselhaus SOC strengths ($\theta_{so} = \pi/4$). The junction and magnetic field orientations are set to $\theta_c = 3\pi/4$ and $\varphi_B = \pi/2$, respectively. The green solid line represents the path of the ground-state phase (ϕ_{GS}) as the Zeeman energy is varied. The vertical (horizontal) dashed line marks a possible transition between a TS state supporting a zero-phase edge-like MS (cyan triangle/dot) and one supporting an end Majorana state (magenta square) during which E_Z (ϕ) is kept constant while ϕ (E_Z) is tuned. A transition between edge-like (e.g., cyan dot) and end-like (e.g., magenta cross) MSs can also be achieved by solely tuning E_Z , as the value of ϕ self-adjusts and follows the path of the ground-state phase (green solid line). (b)-(d) Probability density (normalized to its maximum value) of the MSs corresponding to the E_Z and ϕ values marked in (a) by the cyan triangle (edge-like MS), magenta square (end-like MS), and cyan dot (edge-like MS), respectively. (e)-(g) Energy spectra as a function of the Zeeman energy for $\phi = 0$, $\phi = \pi/2$, and $\phi = 3\pi/5$, respectively. Red-solid and dashed-blue lines represent states that evolve into MSs as E_Z is varied. Vertical dashed lines indicate the boundaries of the first topological region in which only a single pair of MSs (red solid lines) exists.

corresponding to the E_Z and ϕ values indicated by the cyan triangle, magenta square, and cyan dot in Fig. 4 are shown in Figs. 4(b)-(d), respectively. Both the edge-like MSs [Figs. 4(b) and (d)] and the end-like MSs [Fig. 4(c)] exhibit strong localization along the junction direction, resulting in very stable MSs within the first topological region, which contains a single pair of MSs. This stability is evident in the energy spectra presented in Figs. 4(e)-(g) for $\phi = 0, \pi/2, 3\pi/5$, where very flat zero-energy MSs (red lines) with an enhanced topological gap, compared to the cases with only Rashba SOC [see Figs. 2(e)-(g)] or only Dresselhaus SOC [see Figs. 3(e)-(g)], are clearly visible. Notably, the transition between edge-like (cyan dot) and end-like (magenta square) MSs induced by vary-

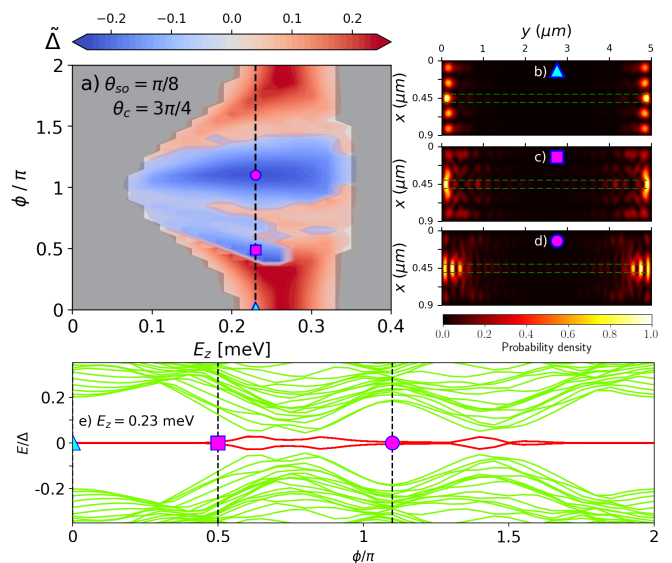


FIG. 5. (a) Topological gap character ($\tilde{\Delta}$) as a function of the Zeeman energy E_Z and the superconducting phase difference (ϕ) across an Al/InSb JJ, with Rashba SOC strength about 2.4 times greater than the Dresselhaus SOC strength ($\theta_{so} = \pi/8$). The junction and magnetic field orientations are set to $\theta_c = 3\pi/4$ and $\varphi_B = \pi/2$, respectively. (b)-(d) Probability density (normalized to its maximum value) of the MSs corresponding to the E_Z and ϕ values marked in (a) by the cyan triangle (edge-like MS), magenta square (end-like MS), and magenta dot (end-like MS), respectively. (e) Energy spectrum along the path indicated by the vertical dashed line in (a), where $E_Z = 0.23$ meV and ϕ is varied from 0 to 2π . The symbols in (e) indicated the energy of the MSs whose probability densities are plotted in (b)-(d).

ing E_Z while keeping $\phi = \pi/2$ is very robust, with MSs maintaining their zero energy and protected by a sizable topological gap, as can be appreciated in Figs. 4(f).

In junctions where the strengths of Rashba and Dresselhaus SOC are equal (e.g., $\theta_{so} = \pi/4$), the topological gap exhibits mirror symmetry with respect to $\phi = \pi$, as shown in Fig. 4(a). However, this symmetry is broken when the Rashba and Dresselhaus SOC strengths are no longer equal, as illustrated in Fig. 5(a), where the topological gap character is plotted as a function of E_Z and ϕ for the case of a JJ with $\theta_{so} = \pi/8$ (i.e., $\alpha/\beta \approx 2.4$), $\theta_c = 3\pi/4$, and $\varphi = \pi/2$. The vertical dashed line highlights a path along which the JJ transitions between end and edge-like MSs as ϕ is varied while keeping E_Z constant. The probability densities of an edge-like MS (cyan triangle) and two end-like MSs (magenta square and magenta dot) are shown in Figs. 5(b)-(d), where their localization properties are illustrated.

The evolution of the energy spectrum along the path marked with the dashed line in Fig. 5(a) is displayed in Fig. 5(e). Red lines represent the energies of the MSs. As the superconducting phase difference is varied, the junction undergoes multiple transitions between end and edge-like MSs. Since all the transitions occur within the

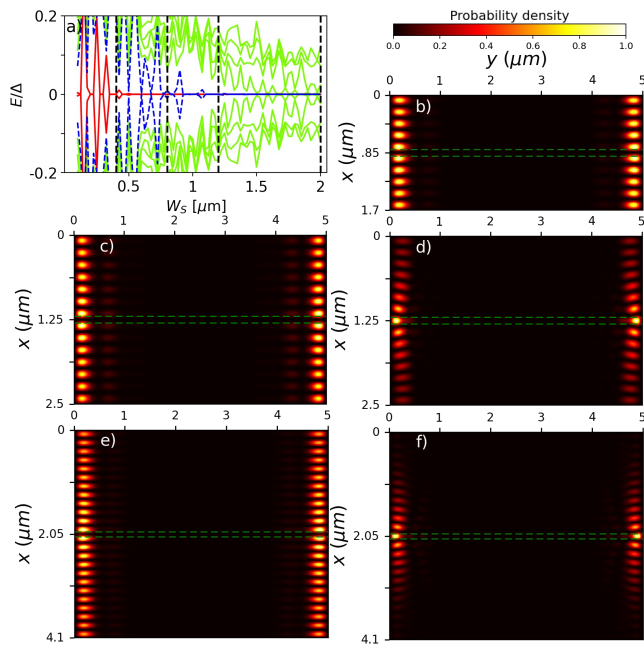


FIG. 6. (a) Energy spectrum as a function of W_S for $\phi = 0$ and $E_Z = 0.25$ meV. The other system parameters were taken as in Fig. 4. Red-solid and dashed-blue lines represent states that evolve into MSs as W_S is varied. Vertical dashed lines indicate W_S -values of $0.4 \mu\text{m}$, $0.8 \mu\text{m}$, $1.2 \mu\text{m}$, and $2 \mu\text{m}$. (b)–(f) Probability density (normalized to its maximum value) for JJs with (b) $W_S = 0.8 \mu\text{m}$, (c) and (d) $W_S = 1.2 \mu\text{m}$, and (e) and (f) $W_S = 2 \mu\text{m}$. The edge-like Majorana pair in (b) evolves into the one shown in (c) (when W_S increases from $W_S = 0.8 \mu\text{m}$ to $W_S = 1.2 \mu\text{m}$) and then into the edge-like pair shown in (e) when $W_S = 2 \mu\text{m}$. A second Majorana pair [shown in (d)] exists when $W_S = 1.2 \mu\text{m}$ and eventually evolves into the end-like MS displayed in (f).

TS state, they occur in a protected way, i.e., without gap closings. This is also true for the transitions indicated in Figs. 2(a), 3(a), and 4(a). It is important to note, however, that for practical applications, the transition path may need to be further optimized with respect to variations in E_Z , ϕ , and system size in order to identify the path between end-like and edge-like MSs that maximizes the topological gap.

To illustrate the behavior of the MSs as the size of the S regions increases, we show in Fig. 6 the energy spectrum as a function of W_S for $\phi = 0$ and $E_Z = 0.25$ meV, with all other system parameters as in Fig. 4. For clarity, only the 12 states with energies closest to zero are shown. Red-solid and blue-dashed lines indicate states that evolve into MSs as W_S increases. In regions where multiple Majorana pairs coexist, some energy lines may be indistinguishable, as they overlap. Vertical dashed-lines mark the values $W_S = 0.4, 0.8, 1.2, 2 \mu\text{m}$.

The probability density (normalized to its maximum value) of the edge-like MSs in a JJ with $W_S = 0.4 \mu\text{m}$ [see Fig. 4(b)] transforms into the edge-like MSs shown in Figs. 6(b), (c), and (e) as W_S increases to $0.8 \mu\text{m}$,

$1.2 \mu\text{m}$, and $2 \mu\text{m}$, respectively. A second Majorana pair appears at $W_S = 1.2 \mu\text{m}$ [see Fig. 6(d)] and eventually transitions into the end-like Majorana pair displayed in Fig. 6(f) as the extent of the S regions increase to $2 \mu\text{m}$. Although not depicted in Fig. 6, a third pair of MSs exists at $W_S = 2 \mu\text{m}$.

It is important to note that as long as the chemical potential μ is larger than the other characteristic energy scales of the system (Δ_0 , E_Z , and the spin-orbit coupling energy splitting), its specific value has no direct impact on the emergence of edge-like Majorana states (MSs), as suggested by Eq. (19). Thus, our calculations for $\mu = 1$ meV (a value larger than the other relevant energy scales) are expected to remain qualitatively accurate even for higher chemical potentials. However, the chemical potential still plays a crucial role, as it affects the extent of the topological region in the $\phi - E_Z$ parameter space. For MSs to emerge, the system must first be driven into the topological superconducting (TS) state. Once in the TS state, the primary effect of the chemical potential is to modulate the oscillations of the edge-like MSs.

As indicated by Eq. (19), when the wave vectors are real, they increase with the chemical potential, leading to shorter wavelengths for the propagating modes and faster oscillations in the probability density of the edge-like MSs. This behavior is evident in Figs. 7(a)–(d), which display the probability density for junctions with chemical potentials of 4 meV, 6 meV, 12 meV, and 15 meV, respectively.

Due to their distinct localization characteristics, end-like and edge-like MSs can yield different experimental outcomes. Understanding the behavior and properties of these states is, therefore, crucial for correctly interpreting their experimental detection. For instance, the sharp contrast in the zero-bias conductance peak (ZBCP) observed in Josephson junctions (JJs) when the superconducting phase is changed from $\phi = 0$ to $\phi = \pi$ [49] could be related to a transition between edge-like and end-like MSs. At $\phi = 0$, edge-like MSs exhibit reduced probability density beneath the contact, leading to a smaller ZBCP amplitude. Conversely, at $\phi = \pi$, end-like MSs have a larger probability density below the contact, resulting in a more prominent ZBCP amplitude. Moreover, because edge-like MSs extend along the entire junction edges, they could act as global interconnects, enabling coupling between distant MSs. This coupling can be controlled by switching between edge-like and end-like MSs, offering a potential mechanism for modulating interactions in topological quantum devices.

IV. SUMMARY

We investigated the formation and properties of edge-like and end-like MSs in proximitized planar JJs subjected to an in-plane magnetic field, considering the effects of Rashba and/or Dresselhaus SOCs. The end-like MSs are primarily localized at opposite ends of the nor-

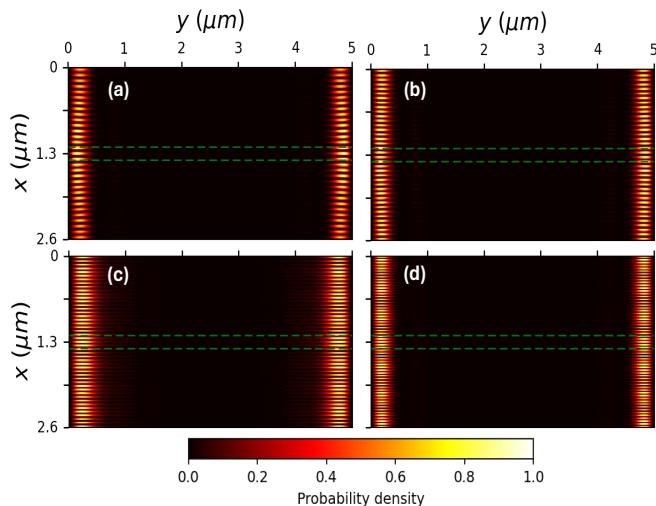


FIG. 7. Probability density (normalized to its maximum value) for JJs with $W_S = 1.2 \mu\text{m}$, $W_N = 0.2 \mu\text{m}$, $E_z = 0.25 \text{ meV}$, and chemical potential (a) $\mu_{S(N)} = 4 \text{ meV}$, (b) $\mu_{S(N)} = 6 \text{ meV}$, (c) $\mu_{S(N)} = 12 \text{ meV}$, and (d) $\mu_{S(N)} = 15 \text{ meV}$. The other parameters were taken as in Fig. 4(a), namely, $\theta_{s_o} = \pi/4$, $\theta_c = 3\pi/4$, $\phi = 0$, and $\varphi_B = \pi/2$.

mal region within the junction. In contrast, the edge-like MSs extend along the system's edges, perpendicular to the junction. To characterize the nature and protection of the MSs we introduced a quantity called the *topological gap character*. This quantity provides insight into whether the system is in the D-class (or BDI-class with \mathbb{Z}_2 index equal to ± 1) TS state, the size of the topological gap, and whether the MSs are end-like or edge-like. Through numerical simulations of the topological gap character as a function of the magnetic field strength and the superconducting phase difference (ϕ) across the junction, we found that when the system is in the TS state, and either Rashba or Dresselhaus SOC dominates, edge-like and end-like MSs, protected by a sizable topological gap, typically emerge near ϕ values of 0 and π , respectively. However, when the Rashba and Dresselhaus SOC strengths are comparable, and the junction and magnetic field are properly oriented, protected edge-like MSs can also emerge at phases near π . Our results reveal the possibility of inducing topologically protected transitions between edge-like and end-like MSs in phase-biased JJs by tuning the superconducting phase difference and the magnetic field strength. Furthermore, in phase-unbiased junctions with comparable Rashba and Dresselhaus SOC strengths, protected transitions between end and edge-like MSs can be achieved by solely adjusting the magnetic field strength, as the superconducting phase self-tunes to minimize the system's free energy. Controlled transitions between edge-like and end-like MSs could function as switchable global interconnects, enabling or disabling the coupling between distant MSs.

ACKNOWLEDGMENTS

A.P.G. is grateful for the funding of PhD scholarship ANID-Chile No. 21210410. P.A.O. acknowledges support from FONDECYT grants 1230933 and 1220700 and USM-Chile under grant PI-LIR-24-10. A.M.-A. acknowledges support from USM-Chile under grant MEC-USM/2023.

Appendix A

The system parameters used in the numerical simulations are listed in Table I. The values of the hopping parameter $t = \hbar^2/(2m^*a^2)$ are also included.

parameter	Al/HgTe [73]	Al/InSb [84]
Δ_0	0.23 meV	0.21 meV
μ_S	1 meV	1 meV
μ_N	1 meV	1 meV
m^*	$0.038m_o$	$0.013m_o$
λ	16 meV nm	15 meV nm
W_N	100 nm	100 nm
W_S	400 nm	400 nm
L	5000 nm	5000 nm
a	10 nm	10 nm
t	10.0 meV	29.3 meV

TABLE I. Material parameters used in the numerical simulations of proximitized planar JJs reported in this work. The proximity-induced superconducting gap is represented by Δ_0 , μ_S (μ_N) denotes the chemical potential in the S (N) region, m^* is the electron effective mass (with m_o as the bare mass of the electron), $\lambda = \sqrt{\alpha^2 + \beta^2}$ characterizes the combined strength of Rashba (α) and Dresselhaus (β) SOC, W_N (W_S) is the width of the N (S) region, L is the length of the junction, a is the TB lattice constant, and t the TB hopping parameter.

Appendix B

To get qualitative insight into the role of the superconducting phase difference in the formation of edge-like and end-like MSs, we assume, without loss of generality that $0 \leq \phi \leq \pi$, consider the BdG Hamiltonian in Eq. (1), and apply the unitary transformation,

$$U = (\tau_0 \otimes \sigma_0) \cos[\text{sgn}(x)\phi/2] + i(\tau_z \otimes \sigma_0) \sin[\text{sgn}(x)\phi/2] \quad (\text{B1})$$

which eliminates the phase dependence of superconducting pairing potential at the expense of adding a phase-dependent gauge field to the x component of the momentum. The transformed Hamiltonian,

$$H' = U^\dagger H U, \quad (\text{B2})$$

has the same form as H but with the original pairing potential in Eq. (6) replaced by the zero-phase pairing,

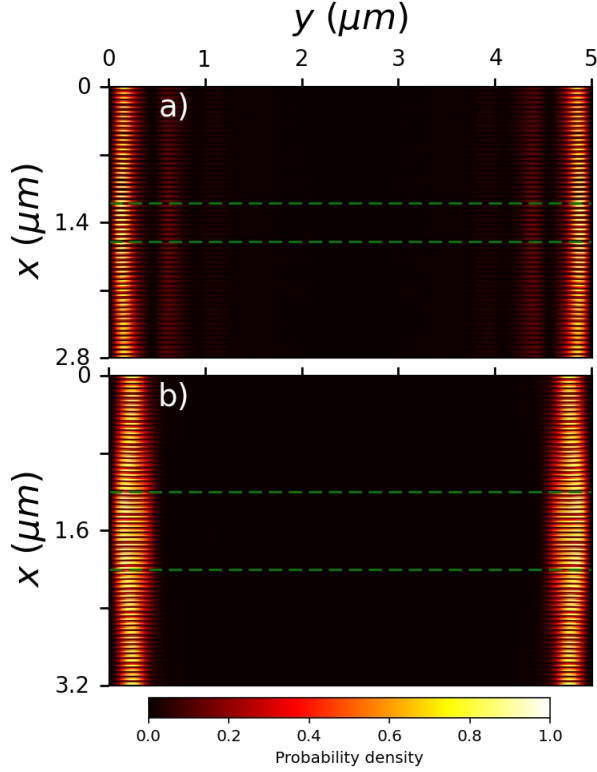


FIG. 8. Probability density (normalized to its maximum value) for JJs with (a) $W_N = 0.4 \mu\text{m}$ and (b) $W_N = 0.8 \mu\text{m}$. The other parameters were taken as in Fig. 7(c), namely, $W_S = 1.2 \mu\text{m}$, $E_Z = 0.25 \text{ meV}$, $\theta_{so} = \pi/4$, $\theta_c = 3\pi/4$, $\phi = 0$, and $\varphi_B = \pi/2$.

$\Delta' = \Delta_0 \Theta(|x| - W_N/2)$, and the momentum component along the x-axis replaced by, $p'_x = p_x \pm (\phi/2)\delta(x)$ in the particle-like (+) and hole-like (-) blocks of the Hamiltonian, respectively. In other words, a JJ with superconducting phase difference ϕ is equivalent to a JJ with zero phase ($\phi = 0$), but with the Dirac function gauge potentials $A_x = \pm (\phi/2)\delta(x)$ acting on the particle-like and hole-like components of the wavefunction. In the case of a JJ with only Rashba SOC, the gauge potential behaves as an attractive potential in the x-direction. Since it is centered in the middle of the normal (N) region, this potential contributes to the localization of the MSs near the ends of the junction. Conversely, when the gauge potential vanishes for $\phi = 0$, the MSs extend along the edges perpendicular to the junction.

Let's now analyze the case in which the Zeeman field dominates the SOC and the spin is approximately conserved. In such a case one can make the approximation $(\mathbf{w} \cdot \mathbf{E}_z)^2 \approx (\mathbf{w} \cdot \mathbf{w})^2 |\mathbf{E}_z|^2$ in Eq. (11) and find approximate analytical solutions for the wave vectors.

1. Magnetic field along the junction ($\mathbf{E}_Z \parallel \hat{y}$)

Consider a magnetic field aligned along the junction, together with the absence of Dresselhaus SOC ($\beta = 0$) or a junction orientation at an odd multiple of $\pi/4$ with respect to the [100] crystallographic direction of the host semiconductor.

The wave vectors at $\phi = 0$ of zero-energy states are given by,

$$q_{j,\pm} = \sqrt{\left[\frac{\sqrt{2m^* (\mu_S + j\sqrt{E_Z^2 - \Delta_0^2})}}{\hbar} \pm k_{so} \right]^2 + \kappa^2} \quad (\text{B3})$$

where $j = e = 1$ ($j = h = -1$) for electron-like (hole-like) states, $E_Z = |\mathbf{E}_Z|$, and

$$k_{so} = \frac{m^* (\alpha + \beta \sin 2\theta_c)}{\hbar^2}. \quad (\text{B4})$$

From Eq. (B3), one finds that the wave vectors are real if,

$$E_Z \geq \Delta_0 \text{ and } \mu_S \geq \sqrt{E_Z^2 - \Delta_0^2}. \quad (\text{B5})$$

Hence, edge-like MSs emerge when the system is in the TS state and the conditions in Eq. (B5) are met. Note that, in principle, for the wavefunction to be delocalized, it is sufficient only one, not all, of the wave vectors to be real. In this case, only the first inequality in Eq. (B5) is required. However, when all the wave vectors are real, the wavefunction is guaranteed to be strongly delocalized.

2. Magnetic field perpendicular to the junction ($\mathbf{E}_Z \perp \hat{y}$)

In this case, the wave vectors of zero-energy states at $\phi = 0$ are found to have the same form as in Eq. (B3) but with,

$$k_{so} = -\frac{m^* \beta \cos 2\theta_c}{\hbar^2}. \quad (\text{B6})$$

We then conclude that in this case, edge-like MSs emerge when the system is in the TS state and the conditions in Eq. (B5) are met.

Appendix C

In Sec. III we focused our discussion on narrow junctions with $W_N = 0.1 \mu\text{m}$ [Figs. 3-6] and $W_N = 0.2 \mu\text{m}$. However, the existence of edge-like MSs is also supported in wider junctions as evidenced by Fig. 8, where the probability density (normalized to its maximum value) is shown for (a) $W_N = 0.4 \mu\text{m}$ and (b) $W_N = 0.8 \mu\text{m}$. The other system parameters were taken as in Fig. 7(c).

-
- [1] A. Y. Kitaev, *Physics-uspekhi* **44**, 131 (2001).
- [2] A. Y. Kitaev, *Annals of physics* **303**, 2 (2003).
- [3] X.-L. Qi and S.-C. Zhang, *Reviews of Modern Physics* **83**, 1057 (2011).
- [4] M. Leijnse and K. Flensberg, *Semiconductor Science and Technology* **27**, 124003 (2012).
- [5] C. Beenakker, *Annu. Rev. Condens. Matter Phys.* **4**, 113 (2013).
- [6] R. Aguado, *La Rivista del Nuovo Cimento* **40**, 523 (2017).
- [7] D. A. Ivanov, *Physical review letters* **86**, 268 (2001).
- [8] C. Nayak, S. H. Simon, A. Stern, M. Freedman, and S. D. Sarma, *Reviews of Modern Physics* **80**, 1083 (2008).
- [9] J. Alicea, Y. Oreg, G. Refael, F. Von Oppen, and M. P. Fisher, *Nature Physics* **7**, 412 (2011).
- [10] D. Aasen, M. Hell, R. V. Mishmash, A. Higginbotham, J. Danon, M. Leijnse, T. S. Jespersen, J. A. Folk, C. M. Marcus, K. Flensberg, *et al.*, *Physical Review X* **6**, 031016 (2016).
- [11] Y. Oreg, G. Refael, and F. von Oppen, *Phys. Rev. Lett.* **105**, 177002 (2010).
- [12] J. D. Sau, S. Tewari, R. M. Lutchyn, T. D. Stanescu, and S. Das Sarma, *Phys. Rev. B* **82**, 214509 (2010).
- [13] J. D. Sau, R. M. Lutchyn, S. Tewari, and S. Das Sarma, *Phys. Rev. Lett.* **104**, 040502 (2010).
- [14] R. M. Lutchyn, J. D. Sau, and S. Das Sarma, *Phys. Rev. Lett.* **105**, 077001 (2010).
- [15] L. P. Rokhinson, X. Liu, and J. K. Furdyna, *Nature Physics* **8**, 795 (2012).
- [16] F. Pientka, G. Kells, A. Romito, P. W. Brouwer, and F. von Oppen, *Phys. Rev. Lett.* **109**, 227006 (2012).
- [17] V. Mourik, K. Zuo, S. M. Frolov, S. Plissard, E. P. Bakkers, and L. P. Kouwenhoven, *Science* **336**, 1003 (2012).
- [18] A. Das, Y. Ronen, Y. Most, Y. Oreg, M. Heiblum, and H. Shtrikman, *Nature Physics* **8**, 887 (2012).
- [19] M. Deng, C. Yu, G. Huang, M. Larsson, P. Caroff, and H. Xu, *Nano letters* **12**, 6414 (2012).
- [20] M. Deng, S. Vaitiekėnas, E. B. Hansen, J. Danon, M. Leijnse, K. Flensberg, J. Nygård, P. Krogstrup, and C. M. Marcus, *Science* **354**, 1557 (2016).
- [21] S. Manna, P. Wei, Y. Xie, K. T. Law, P. A. Lee, and J. S. Moodera, *Proceedings of the National Academy of Sciences* **117**, 8775 (2020).
- [22] J. Klinovaja, P. Stano, and D. Loss, *Phys. Rev. Lett.* **109**, 236801 (2012).
- [23] M. Kjaergaard, K. Wölms, and K. Flensberg, *Phys. Rev. B* **85**, 020503 (2012).
- [24] G. L. Fatim, A. Matos-Abiague, B. Scharf, and I. Žutić, *Phys. Rev. Lett.* **117**, 077002 (2016).
- [25] A. Matos-Abiague, J. Shabani, A. D. Kent, G. L. Fatim, B. Scharf, and I. Žutić, *Solid State Communications* **262**, 1 (2017).
- [26] N. Mohanta, T. Zhou, J.-W. Xu, J. E. Han, A. D. Kent, J. Shabani, I. Žutić, and A. Matos-Abiague, *Phys. Rev. Appl.* **12**, 034048 (2019).
- [27] T. Zhou, N. Mohanta, J. E. Han, A. Matos-Abiague, and I. Žutić, *Phys. Rev. B* **99**, 134505 (2019).
- [28] P. Marra and M. Cuoco, *Phys. Rev. B* **95**, 140504 (2017).
- [29] M. Desjardins, L. Contamin, M. Delbecq, M. Dartiailh, L. Bruhat, T. Cubaynes, J. Viennot, F. Mallet, S. Rohart, A. Thiaville, *et al.*, *Nature materials* **18**, 1060 (2019).
- [30] D. Steffensen, B. M. Andersen, and P. Kotetes, *Phys. Rev. B* **104**, 174502 (2021).
- [31] P. Marra, *Journal of Applied Physics* **132**, 231101 (2022).
- [32] U. Güngördü and A. A. Kovalev, *Journal of Applied Physics* **132**, 041101 (2022).
- [33] T.-P. Choy, J. M. Edge, A. R. Akhmerov, and C. W. J. Beenakker, *Phys. Rev. B* **84**, 195442 (2011).
- [34] I. Martin and A. F. Morpurgo, *Phys. Rev. B* **85**, 144505 (2012).
- [35] F. Pientka, L. I. Glazman, and F. von Oppen, *Phys. Rev. B* **88**, 155420 (2013).
- [36] S. Nadj-Perge, I. K. Drozdov, B. A. Bernevig, and A. Yazdani, *Phys. Rev. B* **88**, 020407 (2013).
- [37] S. Nadj-Perge, I. K. Drozdov, J. Li, H. Chen, S. Jeon, J. Seo, A. H. MacDonald, B. A. Bernevig, and A. Yazdani, *Science* **346**, 602 (2014).
- [38] R. Pawlak, M. Kisiel, J. Klinovaja, T. Meier, S. Kawai, T. Glatzel, D. Loss, and E. Meyer, *npj Quantum Information* **2**, 1 (2016).
- [39] T. Kontos, M. Aprili, J. Lesueur, F. Genêt, B. Stephanidis, and R. Boursier, *Phys. Rev. Lett.* **89**, 137007 (2002).
- [40] F. Pientka, A. Keselman, E. Berg, A. Yacoby, A. Stern, and B. I. Halperin, *Phys. Rev. X* **7**, 021032 (2017).
- [41] D. Pekker, C.-Y. Hou, V. E. Manucharyan, and E. Demler, *Phys. Rev. Lett.* **111**, 107007 (2013).
- [42] M. Hell, M. Leijnse, and K. Flensberg, *Phys. Rev. Lett.* **118**, 107701 (2017).
- [43] F. Setiawan, A. Stern, and E. Berg, *Phys. Rev. B* **99**, 220506 (2019).
- [44] F. Setiawan, C.-T. Wu, and K. Levin, *Phys. Rev. B* **99**, 174511 (2019).
- [45] T. Yokoyama, M. Eto, and Y. V. Nazarov, *Phys. Rev. B* **89**, 195407 (2014).
- [46] A. Fornieri, A. M. Whiticar, F. Setiawan, E. Portolés, A. C. Drachmann, A. Keselman, S. Gronin, C. Thomas, T. Wang, R. Kallagher, *et al.*, *Nature* **569**, 89 (2019).
- [47] H. Ren, F. Pientka, S. Hart, A. T. Pierce, M. Kosowsky, L. Lunczer, R. Schlereth, B. Scharf, E. M. Hankiewicz, L. W. Molenkamp, *et al.*, *Nature* **569**, 93 (2019).
- [48] M. C. Dartiailh, W. Mayer, J. Yuan, K. S. Wickramasinghe, A. Matos-Abiague, I. Žutić, and J. Shabani, *Phys. Rev. Lett.* **126**, 036802 (2021).
- [49] S. Hart, H. Ren, T. Wagner, P. Leubner, M. Mühlbauer, C. Brüne, H. Buhmann, L. W. Molenkamp, and A. Yacoby, *Nature Physics* **10**, 638 (2014).
- [50] T. Laeven, B. Nijholt, M. Wimmer, and A. R. Akhmerov, *Phys. Rev. Lett.* **125**, 086802 (2020).
- [51] A. E. Svetogorov, D. Loss, and J. Klinovaja, *Phys. Rev. B* **103**, L180505 (2021).
- [52] O. Lesser, A. Saydjari, M. Wesson, A. Yacoby, and Y. Oreg, *Proceedings of the National Academy of Sciences* **118**, e2107377118 (2021).
- [53] T. Zhou, M. C. Dartiailh, K. Sardashti, J. E. Han, A. Matos-Abiague, J. Shabani, and I. Žutić, *Nature Communications* **13**, 1738 (2022).
- [54] J. P. T. Stenger, M. Hatridge, S. M. Frolov, and D. Pekker, *Phys. Rev. B* **99**, 035307 (2019).
- [55] J. Cayao, P. San-Jose, A. M. Black-Schaffer, R. Aguado, and E. Prada, *Phys. Rev. B* **96**, 205425 (2017).

- [56] B. Scharf, F. Pientka, H. Ren, A. Yacoby, and E. M. Hankiewicz, *Phys. Rev. B* **99**, 214503 (2019).
- [57] T. Zhou, M. C. Dartiailh, W. Mayer, J. E. Han, A. Matos-Abiague, J. Shabani, and I. Žutić, *Phys. Rev. Lett.* **124**, 137001 (2020).
- [58] Y. Zhang, K. Guo, and J. Liu, *Phys. Rev. B* **102**, 245403 (2020).
- [59] B. D. Woods and T. D. Stanescu, *Phys. Rev. B* **101**, 195435 (2020).
- [60] P. P. Paudel, T. Cole, B. D. Woods, and T. D. Stanescu, *Phys. Rev. B* **104**, 155428 (2021).
- [61] S. Salimian, M. Carrega, I. Verma, V. Zannier, M. P. Nowak, F. Beltram, L. Sorba, and S. Heun, *Applied Physics Letters* **119** (2021).
- [62] F. Setiawan, W. S. Cole, J. D. Sau, and S. Das Sarma, *Phys. Rev. B* **95**, 174515 (2017).
- [63] F. Setiawan and J. Hofmann, *Phys. Rev. Res.* **4**, 043087 (2022).
- [64] A. Banerjee, O. Lesser, M. A. Rahman, H.-R. Wang, M.-R. Li, A. Kringhøj, A. M. Whiticar, A. C. C. Drachmann, C. Thomas, T. Wang, M. J. Manfra, E. Berg, Y. Oreg, A. Stern, and C. M. Marcus, *Phys. Rev. B* **107**, 245304 (2023).
- [65] B. Pekerten, D. Brandão, B. H. Elfeky, T. Zhou, J. E. Han, J. Shabani, and I. Žutić, *Phys. Rev. B* **110**, L060513 (2024).
- [66] B. Pekerten, D. S. Brandão, B. Bussiere, D. Monroe, T. Zhou, J. E. Han, J. Shabani, A. Matos-Abiague, and I. Žutić, *Appl. Phys. Lett.* **124**, 252602 (2024).
- [67] J. D. Pakizer, B. Scharf, and A. Matos-Abiague, *Phys. Rev. Res.* **3**, 013198 (2021).
- [68] B. Pekerten, J. D. Pakizer, B. Hawn, and A. Matos-Abiague, *Phys. Rev. B* **105**, 054504 (2022).
- [69] Y. Tanaka and S. Kashiwaya, *Phys. Rev. B* **56**, 892 (1997).
- [70] Y. Tanaka, Y. Mizuno, T. Yokoyama, K. Yada, and M. Sato, *Phys. Rev. Lett.* **105**, 097002 (2010).
- [71] Y. A. Bychkov and E. I. Rashba, *Journal of physics C: Solid state physics* **17**, 6039 (1984).
- [72] G. Dresselhaus, *Physical Review* **100**, 580 (1955).
- [73] B. Scharf, F. Pientka, H. Ren, A. Yacoby, and E. M. Hankiewicz, *Phys. Rev. B* **99**, 214503 (2019).
- [74] M. Luethi, K. Laubscher, S. Bosco, D. Loss, and J. Klinovaja, *Phys. Rev. B* **107**, 035435 (2023).
- [75] J. D. Sau, R. M. Lutchyn, S. Tewari, and S. Das Sarma, *Phys. Rev. Lett.* **104**, 040502 (2010).
- [76] Y. Nagae, A. P. Schnyder, Y. Tanaka, Y. Asano, and S. Ikegaya, *Phys. Rev. B* **110**, L041110 (2024).
- [77] C.-T. Wu, B. M. Anderson, W.-H. Hsiao, and K. Levin, *Physical Review B* **95**, 014519 (2017).
- [78] B. Lian, X.-Q. Sun, A. Vaezi, X.-L. Qi, and S.-C. Zhang, *Proceedings of the National Academy of Sciences* **115**, 10938 (2018).
- [79] G. C. Ménard, A. Mesaros, C. Brun, F. Debontridder, D. Roditchev, P. Simon, and T. Cren, *Nature communications* **10**, 2587 (2019).
- [80] C. W. J. Beenakker and D. Oriekhov, *SciPost Physics* (2020).
- [81] X. Zhu, *Phys. Rev. B* **97**, 205134 (2018).
- [82] L. Liu, C. Miao, H. Tang, Y.-T. Zhang, and Z. Qiao, *Phys. Rev. B* **109**, 115413 (2024).
- [83] A. Winblad and H. Chen, *Phys. Rev. B* **109**, 205158 (2024).
- [84] W. Mayer, M. C. Dartiailh, J. Yuan, K. S. Wickramasinghe, E. Rossi, and J. Shabani, *Nature communications* **11**, 212 (2020).
- [85] A. P. Schnyder, S. Ryu, A. Furusaki, and A. W. Ludwig, *Physical Review B* **78**, 195125 (2008).
- [86] S. Ryu, A. P. Schnyder, A. Furusaki, and A. W. Ludwig, *New Journal of Physics* **12**, 065010 (2010).
- [87] P. Ghosh, J. D. Sau, S. Tewari, and S. D. Sarma, *Physical Review B* **82**, 184525 (2010).
- [88] S. Tewari and J. D. Sau, *Phys. Rev. Lett.* **109**, 150408 (2012).
- [89] M.-T. Rieder, P. W. Brouwer, and I. Adagideli, *Physical Review B* **88**, 060509 (2013).
- [90] Í. Adagideli, M. Wimmer, and A. Teker, *Physical Review B* **89**, 144506 (2014).
- [91] B. Pekerten, A. Teker, Ö. Bozat, M. Wimmer, and Í. Adagideli, *Physical Review B* **95**, 064507 (2017).
- [92] T. D. Stanescu, R. M. Lutchyn, and S. D. Sarma, *Physical Review B* **84**, 144522 (2011).
- [93] T. D. Stanescu and S. Tewari, *Journal of Physics: Condensed Matter* **25**, 233201 (2013).
- [94] B. Pekerten, A. M. Bozkurt, and Í. Adagideli, *Physical Review B* **100**, 235455 (2019).
- [95] A. Daido and Y. Yanase, *Phys. Rev. B* **95**, 134507 (2017).
- [96] C. W. Groth, M. Wimmer, A. R. Akhmerov, and X. Waintal, *New Journal of Physics* **16**, 063065 (2014).